J Mater Sci (2010) 45:842–849
DOI 10.1007/s10853-009-4008-4

Effect of silicon content on the microstructure and properties of Fe–Cr–C hardfacing alloys

G. Azimi · M. Shamanian

Received: 4 April 2009 / Accepted: 29 October 2009 / Published online: 12 November 2009

Abstract In this study, the surface of St52 steel was alloyed with preplaced powders 55Fe39Cr6C, 49Fe39Cr6C6Si, and 45Fe39Cr6C10Si using a tungsten-inert gas as the heat source. Following surface alloying, conventional characterization techniques, such as optical microscopy, scanning electron microscopy, and X-ray diffraction were employed to study the microstructure of the alloyed surface. Microhardness measurements were performed across the alloyed zone. Room-temperature dry sliding wear tests were used to compare the coatings in terms of their tribological behavior. It was found that the as-deposited coatings contained higher volume fractions of carbides (Cr_7C_3). The presence of 6%Si in the preplaced powders caused an increase in microhardness and wear resistance.

Introduction

Surface coating is employed to increase the wear and corrosion resistance of steels. Coating (hardfacing) applications for wear control vary widely, ranging from very severe abrasive wear service conditions such as rock crushing and pulverizing to applications to minimize metal-to-metal wear, such as control valves, where wear as slight as a few thousandths of an inch is intolerable [1].

G. Azimi
Educational Workshop Center, Isfahan University of Technology (IUT), Isfahan 8415683111, Iran

M. Shamanian (✉)
Department of Materials Engineering, Isfahan University of Technology (IUT), Isfahan 8415683111, Iran
e-mail: shamanian@cc.iut.ac.ir

There are various surface coating techniques, such as nitrocarburizing, plasma nitriding, spark discharging or cladding, hardfacing, and chemical and physical vapor deposition processes [2–7]. Coatings with filler metals or powders are mostly made by welding, thermal spraying, or allied welding processes [1]. In recent years, several studies have been conducted on the gas tungsten arc welding (GTAW) process to modify the properties of steel surface [8–12]. This surface modification by means of cladding and alloying is a process in which an alloy powder of a desirable composition and a thin surface layer of the substrate material are simultaneously melted and then rapidly solidified to form a dense coating, metallurgically bonded to the substrate. Wang et al. [8] produced wear-resistant clad layers on medium-carbon steel by GTAW, where WC and TiC particles were directly added to the specified metal powders. The results showed that the TiC with WC clad layer had a superior wear performance under low sliding speed conditions. Eroğlu et al. [9] investigated the tungsten-inert gas (TIG) surface alloying with preplaced graphite, chromium, and high carbon-ferro-chromium powders on SAE1020 low-carbon steel. Buytoz et al. [10, 11] studied the effect of GTAW parameters on the microstructure properties of SiC-based hardfacing on low alloy steels. They found that the microstructure of the cladding layer was M_7C_3 primary carbides, Fe_3Si, SiC, and the graphitic carbon precipitates. All these indicated that GTAW cladding coatings provide remarkable enhancements in corrosion resistance, wear resistance, and thermal conductivity without impairing bulk properties.

Iron-based alloy coatings have been used widely due to their higher hardness and wear resistance, especially their lower cost compared to nickel-based and cobalt-based alloy coatings [13–16]. Over the past few years, efforts have always been focused on the Fe–Cr–C system [9, 17–19] to

fabricate an in situ Cr_7C_3 carbide-reinforced iron matrix, while fewer studies have been carried out on the Fe–Cr–Si–C system, especially by TIG cladding. In this study, the surface of the St52 steel was intrinsically alloyed with preplaced 55Fe39Cr6C, 49Fe39Cr6C6Si, and 45Fe39Cr6C10Si powders using a tungsten arc heat source under a shield of pure argon gas. Metallographic techniques, energy dispersive spectrograph (EDS), X-ray, and hardness measurements were used to assess composition, microstructure, and hardness of the alloyed zone. Reciprocating wear tests were performed to evaluate wear properties of the alloyed surface. It is expected that the preliminary results can be significant in promoting the development of $Cr_7C_3 + Fe_3Si$ intermetallic reinforced iron matrix composites.

Materials and experimental method

The base metals ($110 \times 40 \times 10$ mm^3) for TIG cladding were prepared from St52 steel plates with the chemical composition given in Table 1. Before cladding, the specimens were ground and cleaned with acetone. Mixtures of Fe, Cr, Si, and graphite powders were used as the cladding materials. The compositions of the powders used for surface alloying are also given in Table 1. To form an alloy filler ($105 \times 30 \times 1.5$ mm^3), a constant high pressure was exerted to the powders. The alloy filler was then placed on the base metal. Table 2 presents the different cladding conditions used in this research.

After surface alloying, samples were cut from the alloyed specimens for microstructural examination and microhardness measurement. The samples were prepared for metallographic examination by grinding on SiC wheels followed by polishing. The coatings were etched by 2% nital, while the base metal was etched by chloride ferric alcohol. Conventional characterization techniques such as optical microscopy, scanning electron microscopy (SEM), EDS, and X-ray diffraction were employed for studying the microstructure and elemental analysis of the alloyed zone. Microhardness values with a 100gr load were taken across the alloyed zone. The dry sliding wear tests at room temperature were performed on a reciprocating wear machine (Center for Tribology, IUT, Isfahan, Iran) in air. The counterpart was AISI 52100 steel ball with a hardness of 63 HRC and a diameter of 3 mm. The wear tests were carried out under a 9 N load at a sliding speed of 0.14 m/s and an amplitude of 8 mm. The friction coefficient was continuously recorded by the tester system. Worn surfaces were analyzed by SEM and the wear volume losses were measured (three replicate tests were conducted for each test condition and the averaged value was recorded).

Table 1 Chemical compositions of the specimen (St52 steel) and powders for surface alloying (wt%)

Chemical component	Fe	C	Si	Mn	Cr
St52 steel	98.29	0.216	0.218	0.951	–
55Fe39Cr6C powder	55	6	–	–	39
49Fe39Cr6C6Si powder	49	6	6	–	39
45Fe39Cr6C10Si powder	45	6	10	–	39

Table 2 GTAW operating parameters

Electrode	W-2% thorium
Diameter	2.4 mm
Electrode polarity	DCEN
Welding current (A)	120
Welding speed (m/s)	1.3×10^{-3}
Argon, flow rate (L/min)	8

Results and discussion

Microstructure characterization

Figure 1 shows the cross-sectional optical micrograph of the clad layers formed by TIG with 54Fe39Cr6C (Fig. 1a), 49Fe39Cr6C6Si (Fig. 1b), and 49Fe39Cr6C10Si (Fig. 1c) powder mixtures. It is evident that the clad layers are adherent, crack/defect free, and consist of two zones comprising a columnar morphology followed by a dendritic structure.

Clad layer thicknesses varied over 2–2.2 mm under the TIG surface cladding (TSC) described above (Table 1). The difference in clad thickness deposit was due to the manual cladding process. Variation of the etching contrast suggests that partial melting of the substrate and intermixing could not be avoided during TSC. A thin white layer was observed on the interface, which indicates good metallurgical bonding between the deposited coating and the substrate.

At the bonding zone, an extremely high rate of heat transfer occurred between the molten pool and the substrate under cooling due to the substrate, which led to a very high rate of solidification. The solid–liquid interface would grow in a flat form giving rise to the formation of a bright flat grain in the coating as shown in Fig. 1.

Figure 2 shows the SEM images of the clad matrix with 55Fe39Cr6C powder mixtures. The microstructure consists of primary austenite and a eutectic phase of austenite and carbides. Using an X-ray diffractometer (Fig. 3) and EDS analysis (Fig. 4), the carbides were identified to be Cr_7C_3, which is in agreement with findings reported in the literature [20–27]. The onset of solidification coincided with the formation of primary austenite while the binary eutectic phase of austenite and Cr_7C_3 transformed from the remaining melt.

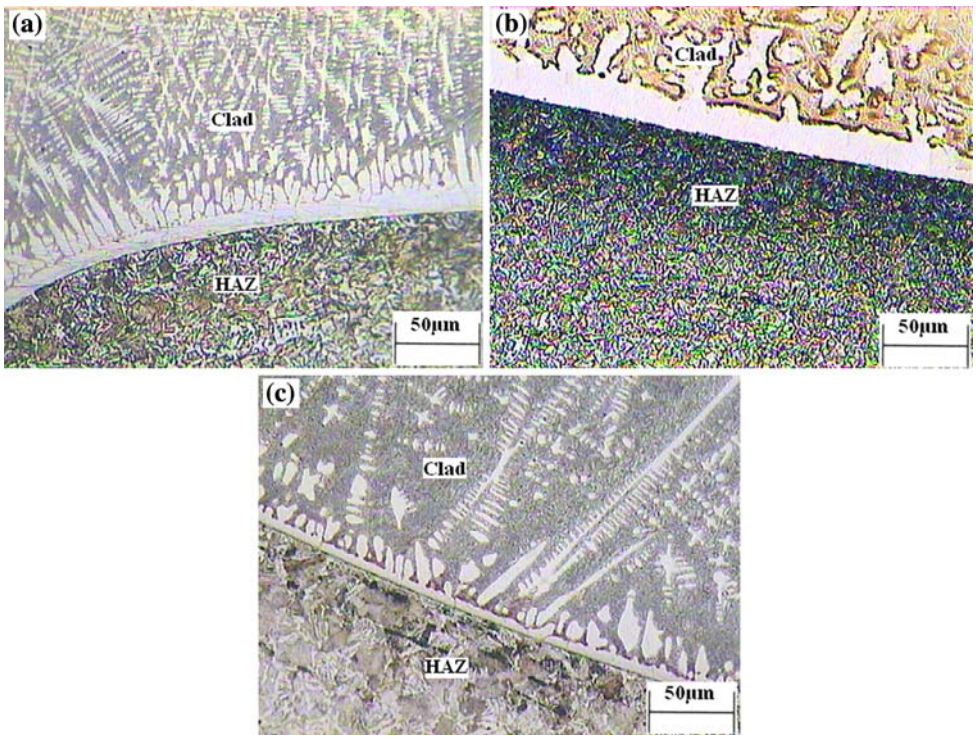

Fig. 1 Cross-sectional optical micrographs of the clad layers formed by GTAW with **a** 55Fe39Cr6C, **b** 49Fe39Cr6C6Si, and **c** 45Fe39Cr6C10Si powder mixtures

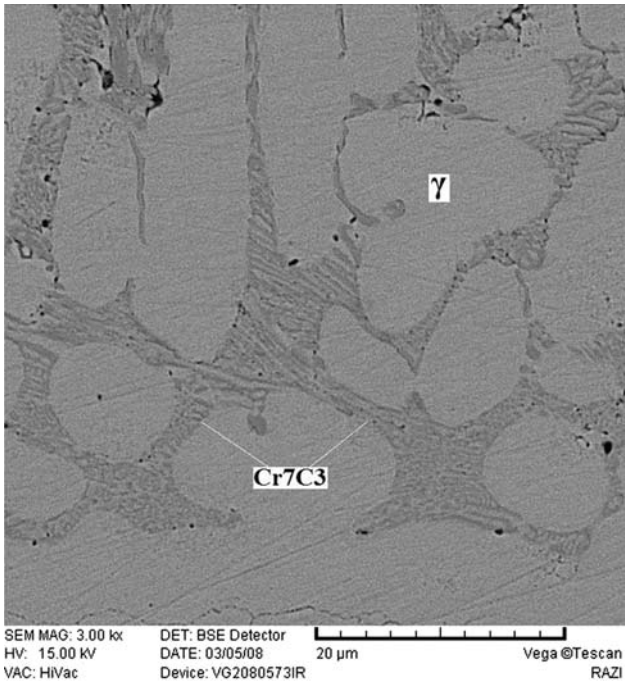

Fig. 2 SEM micrograph of the alloyed zone of the specimen alloyed with 55Fe39Cr6C powder

At room temperature and in the as-solidified condition, both types of austenite (primary and eutectic) were present as retained austenite [20–27]. The details of microstructural investigation of the samples coated by FeCrC powders are given in [28].

The typical microstructure of the TSC with 49Fe39Cr6C6Si powder is shown in Fig. 5. The composite coating consists of a primary phase and a small amount of fine interdendritic eutectic. The primary phase presents a fine dendritic shape. Based on the results obtained from both XRD (Fig. 6) and EDS analyses, the primary phase is identified as austenite and the fine interdendritic eutectic is confirmed to consist of Fe_7C_3, Cr_7C_3 carbides, and the iron-base solid solution γ. It may also be concluded that the iron-based solid solution is saturated with the Si element. In area A (Fe-9.2%Cr-2.4%Si), there is the deposit of dendritic γ-Fe, which is a nonequilibrium phase with an extended solid solution of the alloying elements of Cr and Si, the latter only in small amounts. In area B (Fe-33%Cr-1.4%Si), the eutectic of γ-(Fe,Cr,Si) and carbide is generated. Accompanying the formation of the primary dendritic γ-(Fe,Cr,Si), the residual melt is enriched in carbon and chromium and the eutectic of $\gamma/(Cr,Fe)_7C_3$ is subsequently formed when the concentration in the residual melt reaches a certain level.

Cr_7C_3 carbides are usually covered with another phase, which makes it almost impossible to identify these carbides through the optical microscope [29]. In this study, only Cr_7C_3 could be detected using a back-scattered electron (BSE) image, as shown in Fig. 5.

Figure 6 shows the X-ray diffraction pattern of TIG clad St52 steel with the 49Fe39Cr6C6Si and 45Fe39Cr6C10Si powders. It can be seen that the composite coating consists of γ-Fe, Cr_7C_3, and Fe_7C_3 phases. In the XRD profile, no silicate phase is detected. However, in the case where the

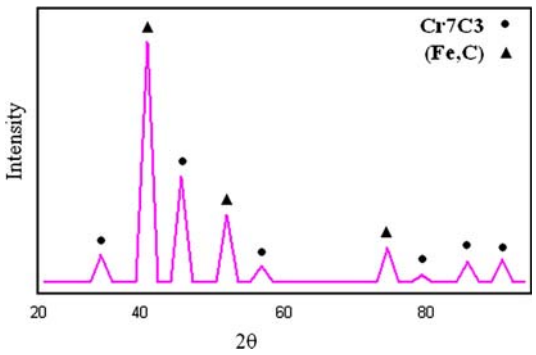

Fig. 3 X-ray diffraction spectrum obtained from the alloyed zone with the 55Fe39Cr6C powder

powder blend for cladding contains 6 wt% Si, Si is detected in EDS analysis of the clad layer. The absence of separate peaks for silicides suggests that Si in the powder blend could have been dissolved in the γ-Fe solid solution [30].

Si is known to have a very low solubility in carbides [31] (and specifically also M_7C_3 [31]). In the case of the surface coating with 49Fe39Cr6C6Si, Si in the powder blend could have been dissolved in the γ-Fe solid solution. Si is found to influence significantly the morphology of M_7C_3 carbides. A further effect of Si is to reduce Cr concentration of the austenite. This is advantageous because Cr is better used in the formation of M_7C_3 carbides [32].

The typical microstructure of TSC with the 45Fe39Cr6C10Si powder is shown in Fig. 7. Results of X-ray diffractometer (XRD), shown in Fig. 6, indicate that the main phases are austenite γ-Fe(Cr,Si) and the compounds Fe_7C_3, Cr_7C_3, and Fe_3Si. The dark area in Fig. 7 represents the deposit of dendritic γ-Fe, which is a non-equilibrium phase with an extended solid solution of the alloying elements Cr and Si, the latter only in small amounts. The bright area in which the eutectic of γ-Fe,

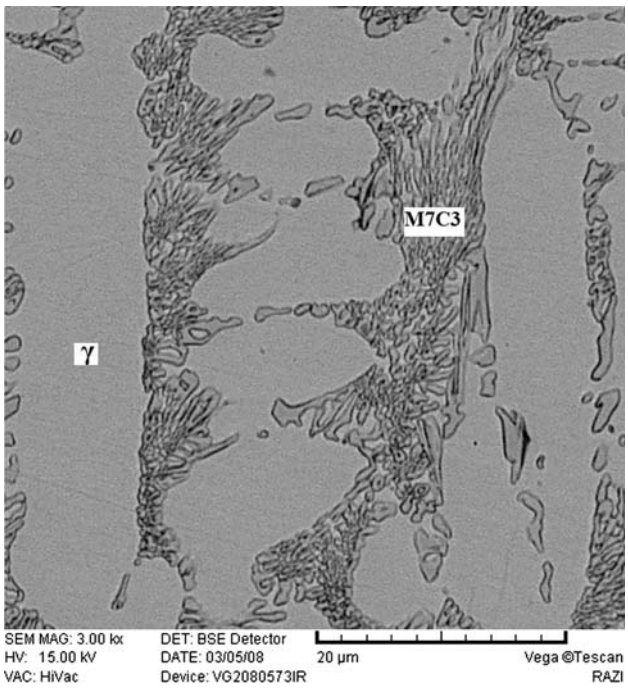

Fig. 5 SEM micrograph of the alloyed zone of the specimen alloyed with the 49Fe39Cr6C6Si powder

carbide, and Fe_3Si were generated, the main elements are Cr, Fe, Si, and C. Accompanying the formation of the primary dendritic γ-Fe, the residual liquid is enriched in carbon, silicon, and chromium, while the eutectic of γ-Fe + alloy carbide and Fe_3Si is subsequently formed when the concentration in the residual liquid reaches a certain level. The carbide and the Fe_3Si are uniformly distributed in the austenite γ-Fe(Cr,Si), as shown in Fig. 7.

The EDS microanalysis shown in Fig. 8 reveals that the coating is principally composed of Si, Cr, and Fe. The atomic percentages obtained from the EDS analysis presented in Fig. 8 and in agreement with phase diagram [33] suggest that the possible phase formed on the surface of

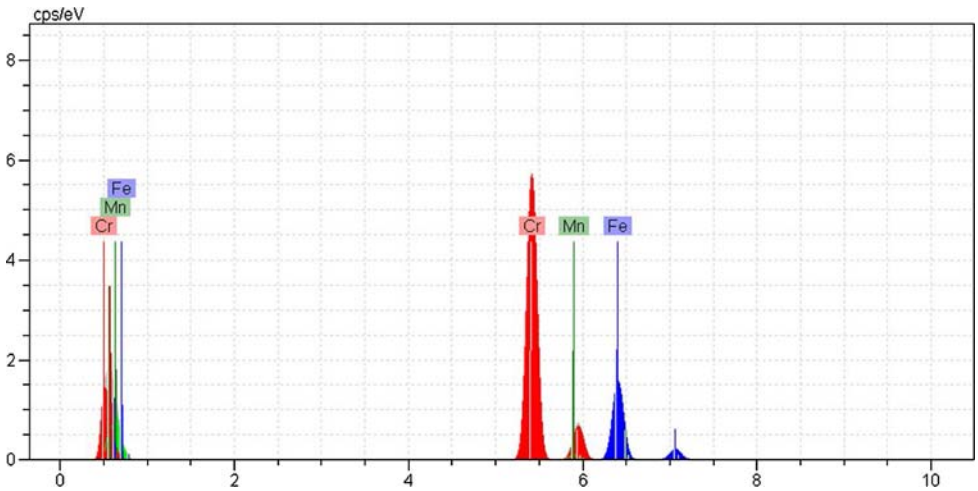

Fig. 4 EDS spectra of the alloyed zone in the specimen alloyed with the 55Fe39Cr6C powder

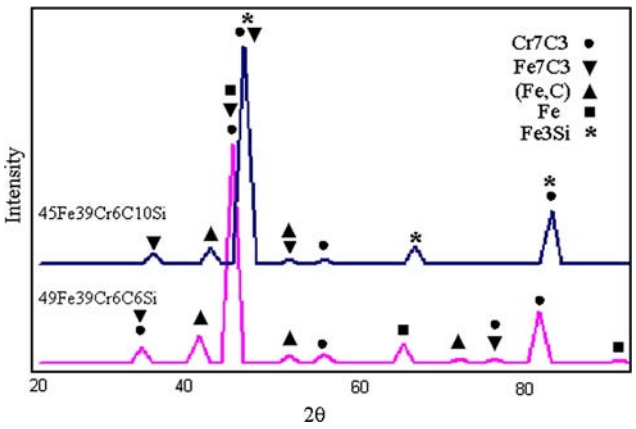

Fig. 6 X-ray diffraction spectrum obtained from the surfaces alloyed with 49Fe39Cr6C6Si and 45Fe39Cr6C10Si powders

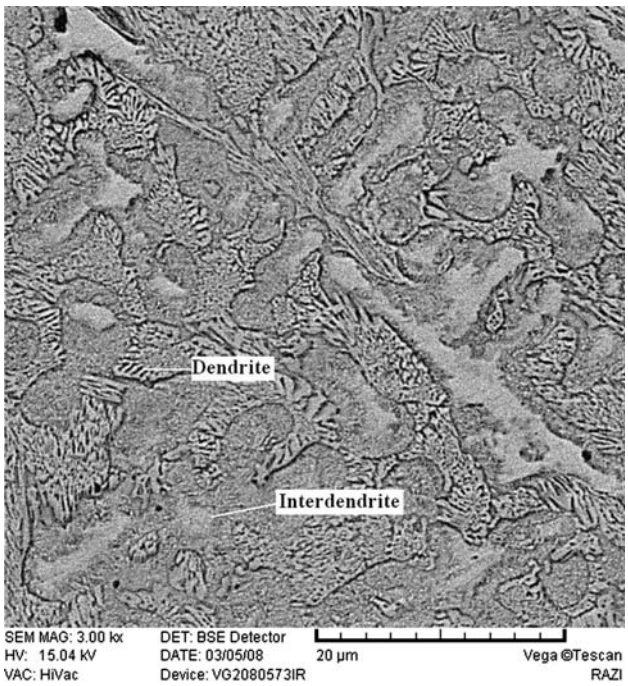

Fig. 7 SEM micrograph of the alloyed zone of the specimen alloyed with the 45Fe39Cr6C10Si powder

steel is Fe_3Si. This was confirmed by the XRD analysis showing the characteristic peaks corresponding to Fe_3Si.

However, phases rich in Si, such as FeSi, are formed at higher temperatures or for longer times and this leads to the formation of a coating that spalls easily [34]. But powders used for this coating consisted of a small amount of Si (10 wt%) while the cooling rate in the welding was high so that the chances for Si-rich silicates to form (such as FeSi and Fe_5Si_3) were very low. This was confirmed by XRD analysis showing the characteristic peaks corresponding to Fe_3Si.

Microhardness of the coatings

Figure 9 presents the microhardness profiles as a function of distance from the surface along the cross-sectional plane for TSC St52 steel with 55Fe39Cr6C, 49Fe39Cr6C6Si, and 45Fe39Cr6C10Si powders. As can be seen in this figure, microhardness significantly increases to above 800 HV as compared to the microhardness value of 200 HV for the as-received substrate. It can be noted that, based on phase analysis, the peak points of the microhardness curves are related to the carbide, while the low points represent the austenite in the coatings [35].

Wear assessment

It can be seen that cladded specimens have lower friction coefficients than the as-received one. The lower coefficient of friction in the coated samples can be explained by the formation of Fe–Cr–C (Fe–Cr–C–Si) coatings having a higher hardness and lower inherent friction characteristic. The effect of higher hardness is to reduce the load transferred to the subsurface, which causes the applied load to be borne mainly by the coating. Thus, the plastic deformation of the subsurface layers decreases and the contact area between the sample and the counterface reduces. As a result, sliding takes place only on very limited asperities at the contact surface. Figure 10 compares the weight loss of the specimens after wear testing. It may be noted that TIG-cladded specimens experienced a significant reduction in wear loss as compared to that in the as-received steel. Additionally, cladding with 49Fe39Cr6C6Si powder was more effective in improving the wear resistance. This improved wear resistance is attributed to the formation of hard carbides (Cr_7C_3, Fe_7C_3) in the microstructure of the solid solution (Fe, Cr, Si) and also to the significant microstructural refinement.

Examination of the surface wear tracks formed after testing was conducted using SEM to identify the predominant wear mechanisms. Figure 11 illustrates the worn surfaces of the coatings. Figure 11a shows the wear tracks formed on the specimen in which cladding was performed with the 55Fe39Cr6C powder. It is observed that the predominant wear mechanism was abrasion with severe ploughing. In other words, the presence of a considerable amount of powder on the surface confirms that the predominant wear mechanism must have been a three-body abrasion wear mechanism. Figure 11b and c shows the wear track formed on the specimens in which cladding was carried out with the 49Fe39Cr6C6Si and 45Fe39Cr6C10Si powders. It is observed here that the predominant wear mechanism was a mild abrasion with ploughing.

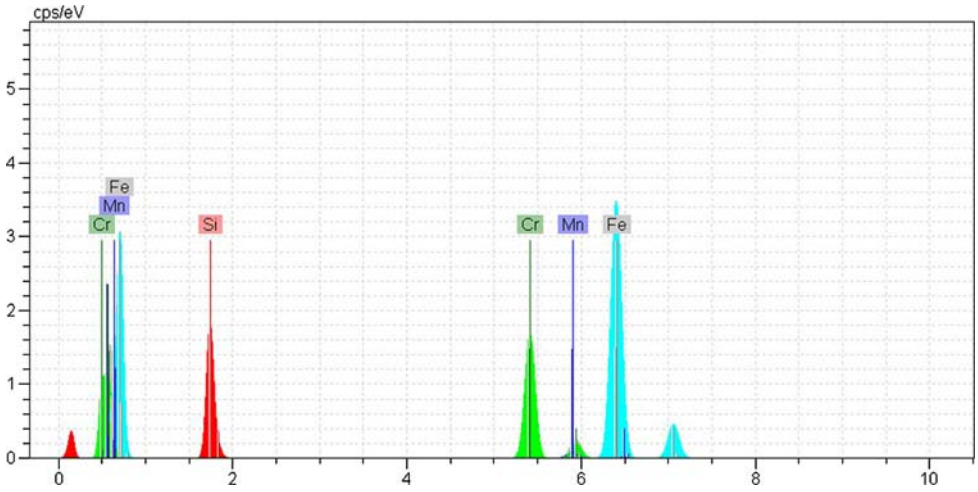

Fig. 8 EDS spectra of the specimen alloyed with the 45Fe39Cr6C10Si powder

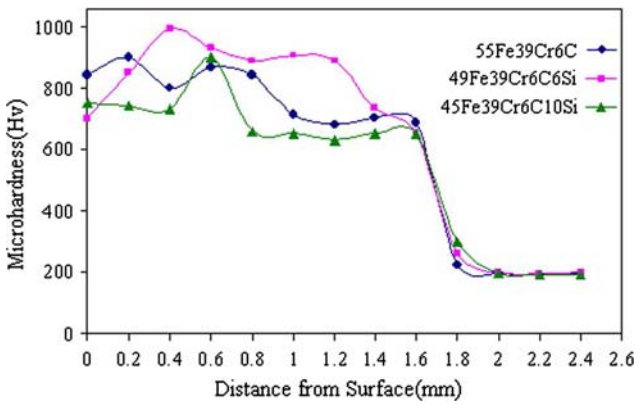

Fig. 9 Microhardness profile of the cladding layers along the cladding layers

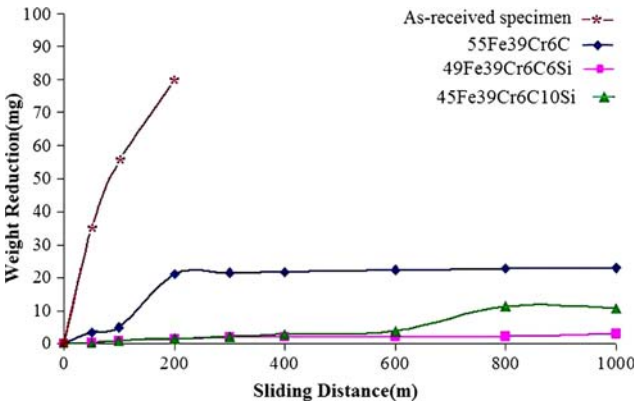

Fig. 10 Weight loss of the as-received and cladded specimens

The clad layer microstructure consists of γ matrix with Cr_7C_3, Fe_7C_3, and Fe_3Si reinforcement particles. In general, the two constituents of the wear-resistant materials serve different functions: the hard particles are to impede wear by grooving or indenting mineral particles, while the metal matrix is meant to provide sufficient toughness. Both properties depend on the amount, size, and distribution of the hard particles as well as on the hardness and fracture toughness of both constituents and the bond between them. A major effect of silicon is to change the morphology of the primary carbides. At very low silicon concentrations, the primary carbides are elongated and tend to become more equiaxed with increasing silicon concentration [32]. These morphological changes should be beneficial to the toughness of the alloy, perhaps imparting better abrasion wear resistance, and in fact, experiments are in progress to confirm this. The effect of Si is also to reduce the level of Cr in the austenite during the eutectic decomposition of the liquid [32]. This may at first sight seem detrimental, but the austenite should in any case decompose eventually to a low-Cr ferrite. The decrease in the Cr content of the austenite formed during solidification should, in fact, be beneficial since Cr is best used in forming hard M_7C_3 carbides during solidification. In fact, Si refines the carbides in the microstructure; such an effect is well established for high-strength steels [32]. At the same time, any change may influence the volume fraction of the hard phase and, thereby, wear properties. This is because the hard particles are to impede wear by grooving or by indenting mineral particles. For these reasons, wear properties and microhardness are improved in surface coating with 49Fe39Cr6C6Si. However, Si content decreases in the austenite, which means that Cr content increases in the austenite in the case of surface coating with 45Fe39Cr6C10Si due to the formation of Fe_3Si. Thus, the possibility for the formation of M_7C_3 decreases, causing microhardness and wear resistance to decline. The results also show that the existence of 6%Si in the coating gives rise to increased microhardness and wear resistance.

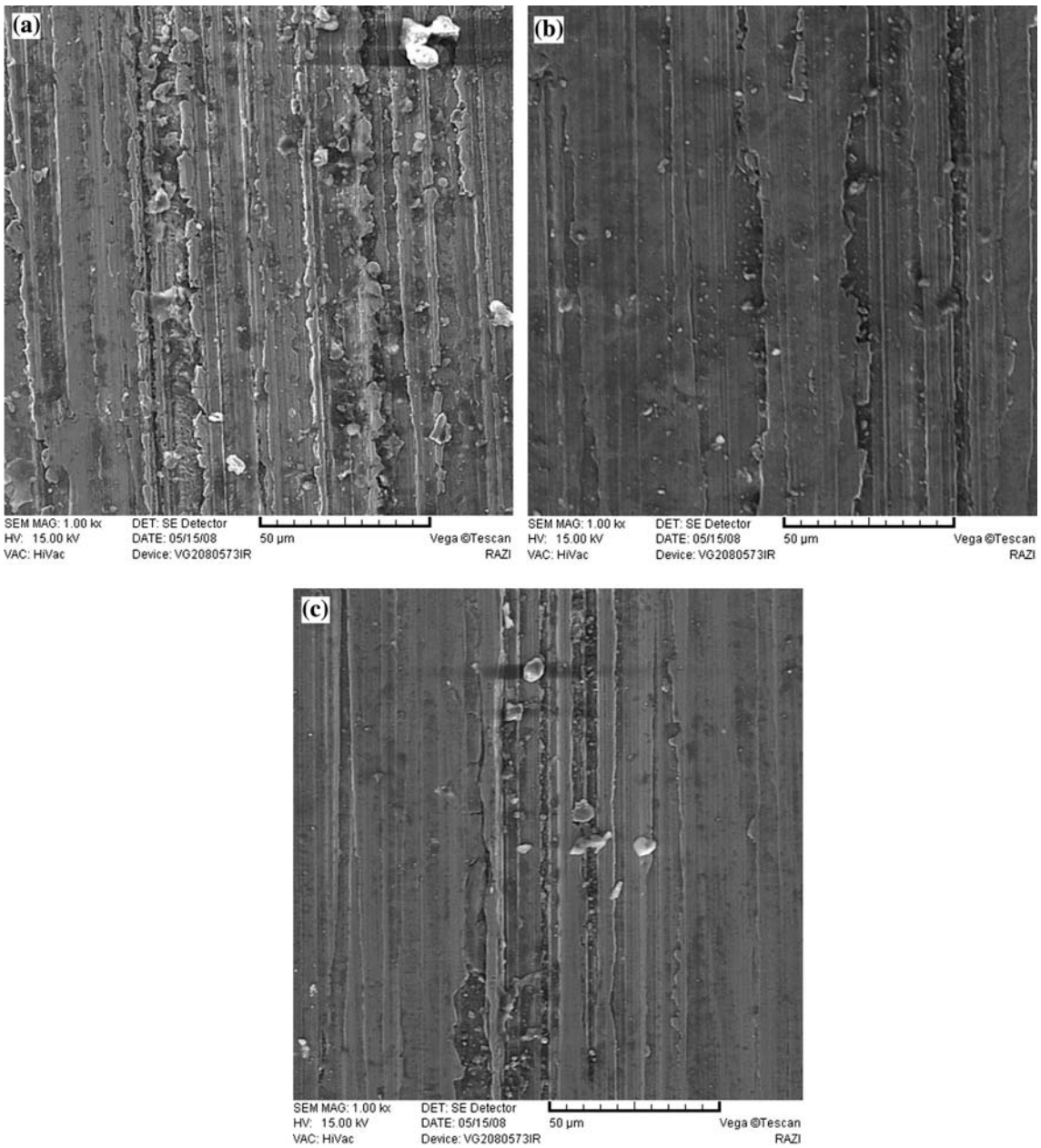

Fig. 11 Micrographs of the worn surfaces after the wear test. **a** 55Fe39Cr6C, **b** 49Fe39Cr6C6Si, **c** 45Fe39Cr6C10Si powders

Conclusions

In this study, Fe–Cr–C and Fe–Cr–Si–C coatings were fabricated on plain carbon steel using the TIG cladding technique. The following conclusions may be drawn from the results obtained:

- Coatings produced by TIG cladding with premixed powders are free from pores or cracks and show good metallurgical bonding with the substrate. The typical coating thickness is about 2–2.5 mm.
- Microhardness exhibits a graded distribution along the depth direction of the cladded coatings. The maximum microhardness value obtained for the cladded coatings is about 980 HV.
- Cladding with 55Fe39Cr6C, 49Fe39Cr6C6Si, and 45Fe39Cr6C10Si powders improve the wear resistance, although cladding with 49Fe39Cr6C6Si is more effective.
- Addition of Si, as the fourth element, to Fe–Cr–C coating is favorable for improving the wear resistance of the coating.

- The presence of 6%Si in the coating increases microhardness and wear resistance.

Acknowledgement The authors wish to thank Isfahan University of Technology (Iran) for their financial support through Grant No. 1MSA851.

References

1. ASM handbook: welding, brazing and soldering, vol 6. ASM International, Materials Park, OH, 1993
2. Li XY (2001) Surf Eng 17:147
3. Qiang YH, Ge SR, Xue QJ (2000) Mater Sci Eng A 278:261
4. Menthe E, Rie KT (1999) Surf Coat Technol 112:217
5. Arnold J, Volz R (1999) J Therm Spray Technol 8:243
6. Haemers TAM, Rickerby DG, Lanza F, Geiger F, Mittemeijer EJ (2000) J Mater Sci 35:5691. doi:10.1023/A:1004858508274
7. Wiklund U, Larsoon M (2000) Wear 241:234
8. Wang SW, Lin YC, Tsai YY (2003) J Mater Process Technol 140:682
9. Eroğlu M, Özdemir N (2002) Surf Coat Technol 154:209
10. Buytoz S, Ulutan M (2006) Surf Coat Technol 200:3698
11. Buytoz S (2006) Surf Coat Technol 200:3734
12. Wang X, Cheng L, Zhang M, Zou Z (2009) Surf Coat Technol 203:976
13. Bourithis L, Papadimitriou G (2003) Mater Lett 57:1835
14. Corbin SF, Toyserkani E, Khajepour A (2003) Mater Sci Eng A 354:48
15. Gatto A, Bassoli E, Fornari M (2004) Surf Coat Technol 187:265
16. D'Oliveira ASCM, Vilar R (2002) Appl Surf Sci 201:154
17. Manna I, Dutta Majumdar J, Ramesh Chandra B, Dahotre NB, Nayak S (2006) Surf Coat Technol 201:434
18. Oh H, Lee S, Ahn S (1992) Metall Mater Trans 33:515
19. Liu Y-F, Xia Z-Y, Han J-M et al (2006) Surf Coat Technol 201:863
20. Pero-Sanz JA, Asensio J (1999) Mater Charact 43:33
21. Izciler M, Celik H (2000) J Mater Process Technol 105:234
22. Arikan MM, Cimenoglu H, Kayali ES (2001) Wear 247:231
23. ASM handbook: heat treating, vol 4. ASM International, Materials Park, OH, 1993
24. Tabrett CP, Sare IR (2000) J Mater Sci 35:2069. doi:10.1023/A:1004755511214
25. Berns H, Fischer A (1997) Mater Charact 39:499
26. Dogan ON, Hawk AJ, Laird G II (1997) Metall Mater Trans A 28:1315
27. Kagawa A, Kawashima S, Ohta Y (1997) Mater Trans A 28:1171
28. Yilmaz O, Ozenbas M, Buytoz S (2002) Mater Sci Technol 18-10:1209
29. Fan C, Wu W, Chang C-M, Chen M-C (2006) Surf Coat Technol 201:908
30. Manna I et al (2006) Surf Coat Technol 201:434
31. Svensson LE, Gretoft B, Ulander B, Bhadeshia HKDH (1986) J Mater Sci 21:1015. doi:10.1007/BF01117388
32. Atamert S, Bhadeshia HKDH (1988) In: Proceedings of international conference on "Heat Treatment '87". Institute of Metals, London, pp 39–43
33. II′Inskii A, Slyusarenko S, Slukhovskii O, Kaban I, Hoyer W (2002) Non-Cryst Solids 306:90
34. Perez Mariano J, Elvira J, Plana F, Colominas C (2006) Surf Coat Technol 200(18/19):5606
35. Zhang L, Liu B, Yu H, Sun D (2007) Surf Coat Technol 201:5931